5th International Conference on Experimental Fluid Mechanics ICEFM 2018 Munich
Munich, Germany, July 2-4, 2018

On the aerodynamic behavior of an airfoil under tailored turbulent inflow conditions

Dominik Traphan[1*], Tom T. B. Wester[1], Joachim Peinke[1], Gerd Gülker[1]

[1] Forwind, Institute of Physics, University of Oldenburg, Oldenburg, Germany

[*] dominik.traphan@uol.de

Abstract

Wind turbines are exposed to multi-scale flow structures contained in the atmospheric boundary layer that manifest as a variety of gusts locally acting on the rotor blades. Particularly aerodynamic principles involved in the interaction of airfoil with three-dimensional unsteady inflows are far from being well understood. On the other hand, flow formation about airfoils in complex inflows is difficult to analyze since chaotic flow appearance obscures relevant connections. The present study thus aims at analyzing an airfoil subjected to a longitudinal and a vertical gust, respectively, by means of the stochastic method called proper orthogonal decomposition (POD). The underlying time series of velocity fields is captured using stereoscopic particle image velocimetry. In both fundamentally different inflow cases, POD analysis shows to retrieve information about total lift evolution from local velocity measurements. Particularly for the vertical gust case, this is remarkable because three-dimensional inflow variation along the span of the airfoil is present. POD thus proves to be a valuable method to uncover additional aerodynamic information in complex flows about airfoils that otherwise remains overlooked.

1 Introduction

Wind turbines are constantly facing the atmospheric boundary layer (ABL) which is characterized by gusts that induce various aerodynamic situations at the rotor within seconds. Such situations often appear as vibrations or dynamic loads at the rotor blades contributing to fatigue of the whole wind turbine (Spinato et al., 2009). Vertical velocity components in the ABL induce chordwise fluctuations in the local inflow velocity at the rotor blade. Such longitudinal gusts have non-linear impact on lift generation, particularly at an angle of attack (AoA) about the stall angle where maximum lift is generated and significant flow separation occurs (Granlund et al., 2014). On the other hand, a gust perpendicular to the rotor plane of a wind turbine locally induces angular variation of inflow at the rotor blade. As a response to rapid changes of AoA, stall of the rotor blade is delayed resulting in a sequence of overshoot and sudden drop in lift. This phenomenon, referred to as dynamic stall (Harris and Pruyn, 1968; Liiva, 1969), is considered as one of the most important sources for dynamic loads at rotor blades of wind turbines. While three-dimensional flow formation about rotor blades as well as dynamic behavior of lifting surfaces under (quasi-) two-dimensional inflow conditions are subject of several studies, the aerodynamic response of lifting surfaces to unsteady three-dimensional inflow raises unsettled issues (Choudhry et al., 2014). Therefore, connections between three-dimensional dynamic inflow, flow formation about an airfoil and its corresponding aerodynamic behavior need to be established. However, realistic inflows resembling properties of the ABL are complex and difficult to comprehend. As a stochastic method, proper orthogonal decomposition (POD) has proven to be useful for extracting essential features from measured velocity fields about airfoils (Bernero and Fiedler, 2000; Melius et al., 2016). The present experimental study thus addresses the question whether POD of the flow about an airfoil subjected to unsteady, three-dimensional inflow is able to uncover relevant aerodynamic connections. The investigated types of inflow simulate two typical inflow situations for wind turbines in the ABL: a longitudinal and a transversal gust.

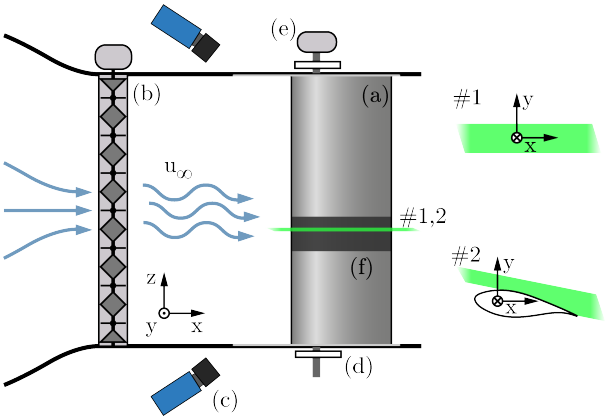

Figure 1: Schematic representation of two setups, #1 and #2, consisting of: (a) vertically mounted DU 91-W2-250 profile with aspect ratio $AR = \mathrm{s/c} = 805\ \mathrm{mm}/300\ \mathrm{mm} \approx 2.68$, view on suction side, (b) active grid in vertical axes excitation mode, (c) two SPIV cameras in stereoscopic configuration #1 and #2, (d) multi-component scale, (e) stepper motors for setting AoA and moving axes of active grid, (f) anti-reflection foil. In configuration #1 the free stream is measured while configuration #2 captures the flow above the airfoil.

2 Methods

Measurements are performed in a closed-return wind tunnel providing Reynolds numbers with respect to the airfoil chord length, c, of up to $Re_c \leq 1 \times 10^6$ at full optical accessibility, see Figure 1. The airfoil under investigation is a DU 91-W2-250 wind profile with an aspect ratio of $AR = s/c = 805\ \mathrm{mm}/300\ \mathrm{mm} \approx 2.68$, where s denotes the span of the airfoil. Streamwise direction corresponds to x, wall-normal direction to y and spanwise direction to z. The coordinate origin is at the intercept of quarter-chord line of the airfoil and center line of the wind tunnel. Hence, quarter chord line is at $x/\mathrm{c} = y/\mathrm{c} = 0$, which is $\Delta x/\mathrm{c} = 3.68$ downstream of the nozzle of the wind tunnel. Aerodynamic performance is quantified by means of a multi-component scale resolving total lift up to a sampling frequency of $f_\mathrm{s} = 1$ kHz limited to eigenfrequencies of the airfoil support.

Inflow is modulated by an active grid featuring rhombic flaps mounted on seven horizontal and nine vertical shafts individually driven by stepper motors. Details about the functionality of the grid are given in Knebel et al. (2011) and Weitemeyer et al. (2013). The specific grid design allows tailoring inflow in time and space. First, a longitudinal gust is generated by quasi stationary motion of the flaps modulating the blockage of the grid. Second, specific sinusoidal motion of the flaps with an excitation frequency of $f_\mathrm{ex} = 5$ Hz yields angular fluctuations in temporal and spanwise directions. The temporal periodicity of $T = 200$ ms follows the excitation frequency while the spatial periodicity in spanwise direction of $\Delta z/c = 0.36$ corresponds to one edgewise flap diameter of the active grid. The maximum phase shift of the inflow $\Delta t_\mathrm{max}/T = 0.24$ is thus observed between the center line and $z/c = 0.18$, as indicated by the arrows representing the inflow downstream of the active grid in Figure 1. The longitudinal and vertical gust cases yield moderate Reynolds numbers of $Re_c = 0.2 \times 10^6$ and $Re_c = 0.4 \times 10^6$, respectively.

The free stream as well as the flow along the suction side of the airfoil are visualized by means of time-resolved stereoscopic particle image velocimetry (SPIV), see configurations #1 and #2 in Figure 1. A measurement frequency of $f_s = 694$ Hz allows 1822 consecutive snapshots that correspond to a total measurement time of $t_\mathrm{tot} \approx 2.6$ s. A spatial resolution of $3 \times 10^{-3} c$ at a sufficient measurement accuracy (i.e. stereo residue < 0.5 px) and a temporal resolution of at least 10 snapshots while flow is advecting over one chord length are obtained.

Since flow formation is complex, relevant flow structures are uncovered by applying snapshot proper orthogonal decomposition (POD) to the velocity fields (Bernero and Fiedler, 2000). Such analysis yields a set of normalized spatial eigenmodes, Φ_i, of the total time series representing spatial coherences ordered by their respective content of energy fluctuations. Each spatial eigenmode is paired with a temporal weighting coefficient, $a_i(t)$. The contribution of a spatial eigenmode to a velocity field at a given time, t, is reflected by the magnitude of its weighting and can thus be followed in time by the time series of $a_i(t)$.

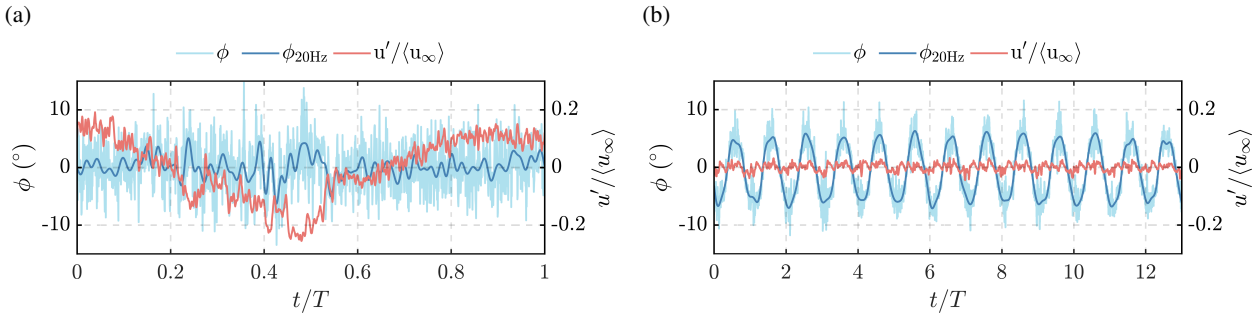

Figure 2: Basic inflow representation of longitudinal gust case in (a) and the periodic vertical gust in (b).

3 Results

The objective of this study is to uncover connections between unsteady, three-dimensional flow formation about an airfoil (locally measured) and resultant total lift generation by means of POD. For this purpose, the two investigated inflow situations are briefly characterized. According to the Reynolds decomposition, fluctuations of a quantity are indicated by $'$. The inflow angle, ϕ, as well as the magnitude of velocity fluctuation, u', are shown as a function of time, t, normalized by the respective period length, T, for both inflow cases in Figure 2. The longitudinal and vertical gust cases in Figures 2a and 2b refer to period lengths of $T_{\parallel} \approx 2.6$ s $= t_{\mathrm{tot}}$ and $T_{\perp} = 0.2$ s, respectively.

The longitudinal gust reveals a velocity decrease of $\Delta u'_{\mathrm{max}}/\langle u_\infty \rangle \approx 0.4$ which is designed following a real gust measured in the ABL (not shown here). The gust contains small-scale turbulence shed by the active grid giving a base line turbulence intensity of $Ti < 3$ %. This also manifests as rapid angular fluctuations ϕ. A low-pass filter with a cutoff frequency of 20 Hz applied to the angular evolution, $\phi(t)$, reflects the effect of spatial filtering caused by the size of the airfoil. Present angular fluctuations with a standard deviation of $\sigma(\phi_{20\mathrm{Hz}}) \approx 1.7°$ thus also affect aerodynamics.

The amplitude of the filtered angular fluctuation of the vertical gust is $|\phi|_{20\mathrm{Hz,max}} \approx 6°$. The associated frequency of $f_{\perp} = 5$ Hz matches the excitation frequency of the active grid. Along with the inflow velocity u_∞, this yields a reduced frequency of $f_{\mathrm{r}} = \pi f_{\perp} c/u_\infty = 0.15$ which corresponds to unsteady aerodynamics (Leishman, 2016). In terms of aerodynamics, the base line turbulence intensity of the velocity magnitude of $Ti < 3$ % is small compared to $|\phi|_{\mathrm{max}}$. Please note that the vertical gust case is three-dimensional implying a spatial periodicity in spanwise direction which is associated with a phase shift of $\Delta t_{\mathrm{max}}/T = 0.24$ between the center line and $z/c = 0.18$. Further inflow measurements are not shown here.

Results on the aerodynamic response of the airfoil to a longitudinal gust are presented below. In Figure 3a, the mean velocity field above the airfoil is depicted for a geometric angle of attack of $\alpha = 10°$ (magnitude of 3D velocity vector is color-coded). The formation of a small wake region close to the trailing edge is observed. To extract relevant features from complex flow formation and relate them to aerodynamic parameters, the time series of velocity fields is analyzed by applying POD based on the velocity fluctuations. An original snap-shot at a given time is thus reconstructed by superposition of the mean velocity field and the normalized eigenmodes, Φ_i, weighted by their associated evolution coefficients, $a_i(t)$. Contributing a turbulent kinetic energy of 54 %, the first spatial POD eigenmode represents inflow variations in terms of velocity magnitude (see Figure 3b). The velocity vectors and color-coded magnitude are depicted normalized. The second eigenmode (see Figure 3c) contains only 4 % of turbulent kinetic energy and reflects increasing boundary layer instabilities as well as the subsequent stall region. In terms of energy, the result of the POD analysis suggests velocity magnitude of inflow as the major aerodynamics governing feature. Indeed, comparing $a_1(t)$ from the first temporal eigenmode against evolution of lift, $F'_{\mathrm{L,tot}}$, as plotted in Figure 3d, shows convincing correlation between the two quantities. The evolution coefficient neither covers small-scale fluctuations nor some details of $F'_{\mathrm{L,tot}}$ about the time $t/T \approx 0.5$. The latter deviation emerges along with significant angular fluctuations (cf. Figure 2a) and thus indicates causality. Missing small-scale fluctuations is considered as expected because the POD is derived from a local SPIV measurement that does not capture all details of the flow formation along the whole span that culminates in total lift.

The vertical gust case is investigated in the same experimental setup and similarly presented as the longitudinal one. Relevant results, i.e. the first spatial eigenmode as well as the comparison of the associated evolution coefficient, $a_1(t)$, with the lift force, $F'_{\mathrm{L,tot}}$, are shown in Figure 4. The formation of a wake region is captured by Φ_1 and contains 56 % of the turbulent kinetic energy, see Figure 4a. By analogy with the

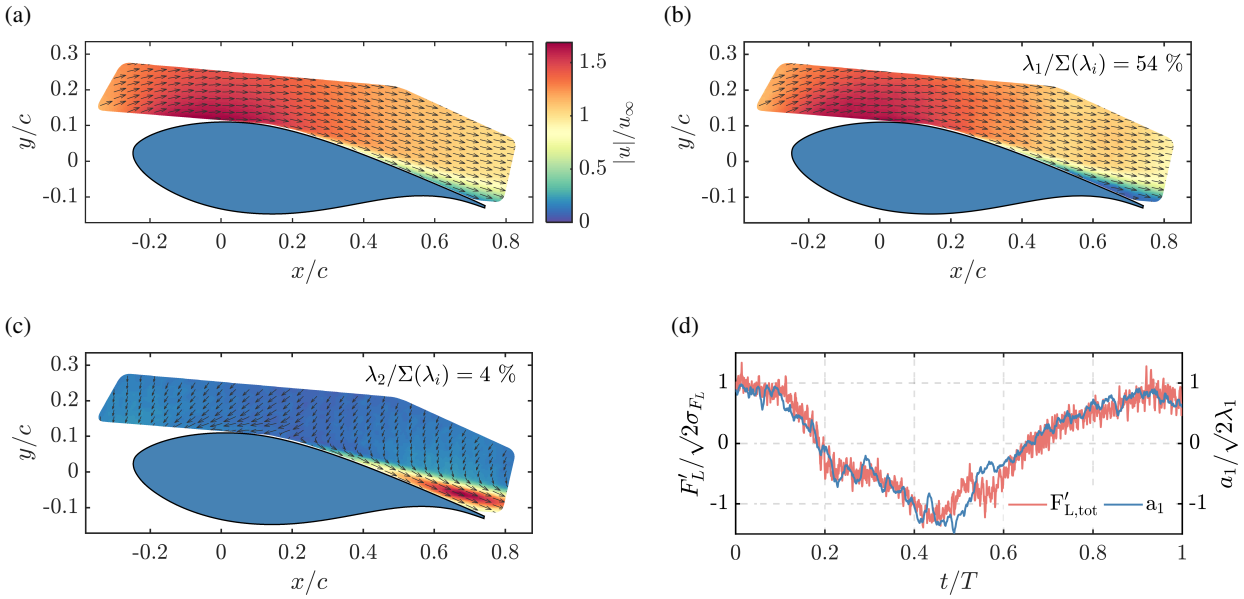

Figure 3: POD of longitudinal gust case consisting of mean velocity field in (a) and the first as well as the second spatial eigenmodes in (b) and (c), respectively. The fluctuations of lift force are compared with the evolution coefficient of the first eigenmode in (d).

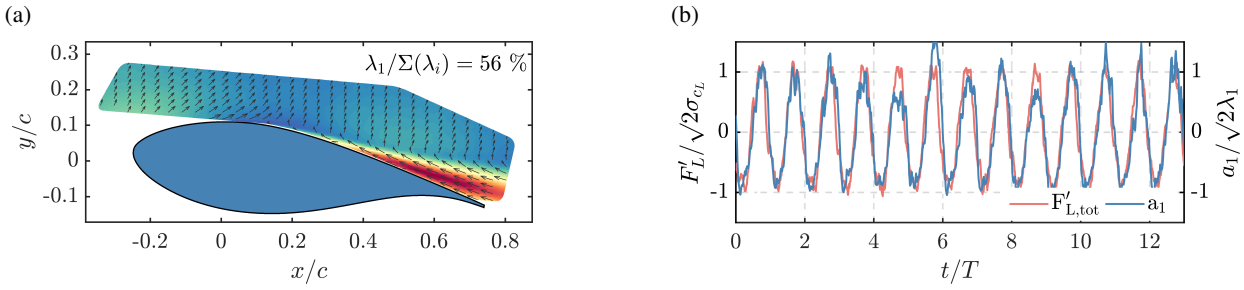

Figure 4: Selected results of POD analysis of the vertical gust case. The first spatial eigenmode is shown in (a). Its associated evolution coefficient is compared against the simultaneous variation in lift force in (b).

first inflow situation, this suggests that the evolution of stall is the major aerodynamics governing feature. Whether this connection also holds true reveals a comparison of the fluctuations of lift force against the first POD evolution coefficient in Figure 4b. Over long periods, such as the first three and the last four cycles, both curves collapse even in details. In some instances, such as fifth and sixth cycle, there are significant deviations. However, the overall similarity is astonishing with respect to the three-dimensional inflow that the airfoil is subjected to along its span.

For the sake of completeness, the mean velocity field as well as the second spatial eigenmode of the vertical gust case are briefly described only. The mean velocity field reveals a slightly larger separation region than observed in the longitudinal gust case, cf. Figure 3a. The second spatial eigenmode captures the inflow in terms of angular fluctuations contributing 10 % to the turbulent kinetic energy. This is in reverse order to the first inflow situation, where inflow variation represents the most energetic part of the flow formation.

4 Conclusion

The present study targets the analysis of complex inflow situations that induce three-dimensional and unsteady aerodynamics at airfoils. A POD analysis of SPIV data of the flow above an airfoil is thus assessed whether results provide valuable insights into the aerodynamic impact of two fundamentally different gusts

that rotor blades of wind turbines typically encounter. In both inflow situations, i.e. a longitudinal gust and a vertical gust with three-dimensional variation along the airfoil span, POD captures dominant aerodynamics in terms of lift generation although POD is derived from local measurements whereas lift is an integrated quantity of the whole airfoil. Particularly considering that the vertical gust contains three-dimensional inflow variation along the span of the airfoil, these results indicate significant value of POD for in depth analysis of complex aerodynamic flow situations.

As a next step, these first promising results should be verified using POD in the context of an aerodynamic phenomenon that is not yet well understood. The vertical gust investigated in this study presents itself as suitable because it is characterized by a reduced frequency that induces three-dimensional dynamic stall. As mentioned in the introduction, the formation of three-dimensional dynamic stall leaves many questions unanswered.

Along with uncovering relevant phenomena in complex aerodynamic flows, obtained results also imply that a POD has the potential to reduce measuring effort. In some aerodynamic flow situations where three-dimensional inflow is involved, a combination of SPIV and POD yields additional information about three-dimensional flow formation based on one local measurement only. Eventually, a POD can be used as a low order model implemented in efficient engineering tools that wind turbine developers use for the design of rotor blades.

Acknowledgements

The authors thank Tim Homeyer for his advice during the experiment. This work is partly funded by the Federal Ministry for Economic Affairs and Energy according to a resolution by the German Federal Parliament (project “Smartblades”) and by the Ministry for Science and Culture of Lower Saxony through the funding initiative “Niedersächsisches Vorab” (project “ventus efficiens”).

References

Bernero S and Fiedler HE (2000) Application of particle image velocimetry and proper orthogonal decomposition to the study of a jet in a counterflow. *Experiments in Fluids* 29:S274–S281

Choudhry A, Leknys R, Arjomandi M, and Kelso R (2014) An insight into the dynamic stall lift characteristics. *Experimental Thermal and Fluid Science* 58:188–208

Granlund K, Monnier B, Ol M, and Williams D (2014) Airfoil longitudinal gust response in separated vs. attached flows. *Physics of Fluids* 26:027103

Harris FD and Pruyn RR (1968) Blade stall – half fact, half fiction. *Journal of the American Helicopter Society* 13:27–48

Knebel P, Kittel A, and Peinke J (2011) Atmospheric wind field conditions generated by active grids. *Experiments in fluids* 51:471–481

Leishman J (2016) *Principles of Helicopter Aerodynamics*. Cambridge University Press

Liiva J (1969) Unsteady aerodynamic and stall effects on helicopter rotor blade airfoil sections.. *Journal of Aircraft* 6:46–51

Melius M, Cal RB, and Mulleners K (2016) Dynamic stall of an experimental wind turbine blade. *Physics of Fluids (1994-present)* 28:034103

Spinato F, Tavner P, Van Bussel G, and Koutoulakos E (2009) Reliability of wind turbine subassemblies. *IET Renewable Power Generation* 3:387–401

Weitemeyer S, Reinke N, Peinke J, and Hölling M (2013) Multi-scale generation of turbulence with fractal grids and an active grid. *Fluid Dynamics Research* 45:061407